Early results of SIGGMA

Bin Liu & the SIGGMA team

National Astronomical Observatories of China

ICISE, Quy Nhon - July 11, 2018

SIGGMA: The Survey of Ionized Gas in the Galaxy, Made with the Arecibo telescope

Yervant Terzian (Cornell)

Bin Liu (NAOC)

Loren Anderson (WVU)

Anish Roshi (NRAO)

Ed Churchwell (UWM)

Robert Minchin (AO)

Travis McIntyre (UNM)

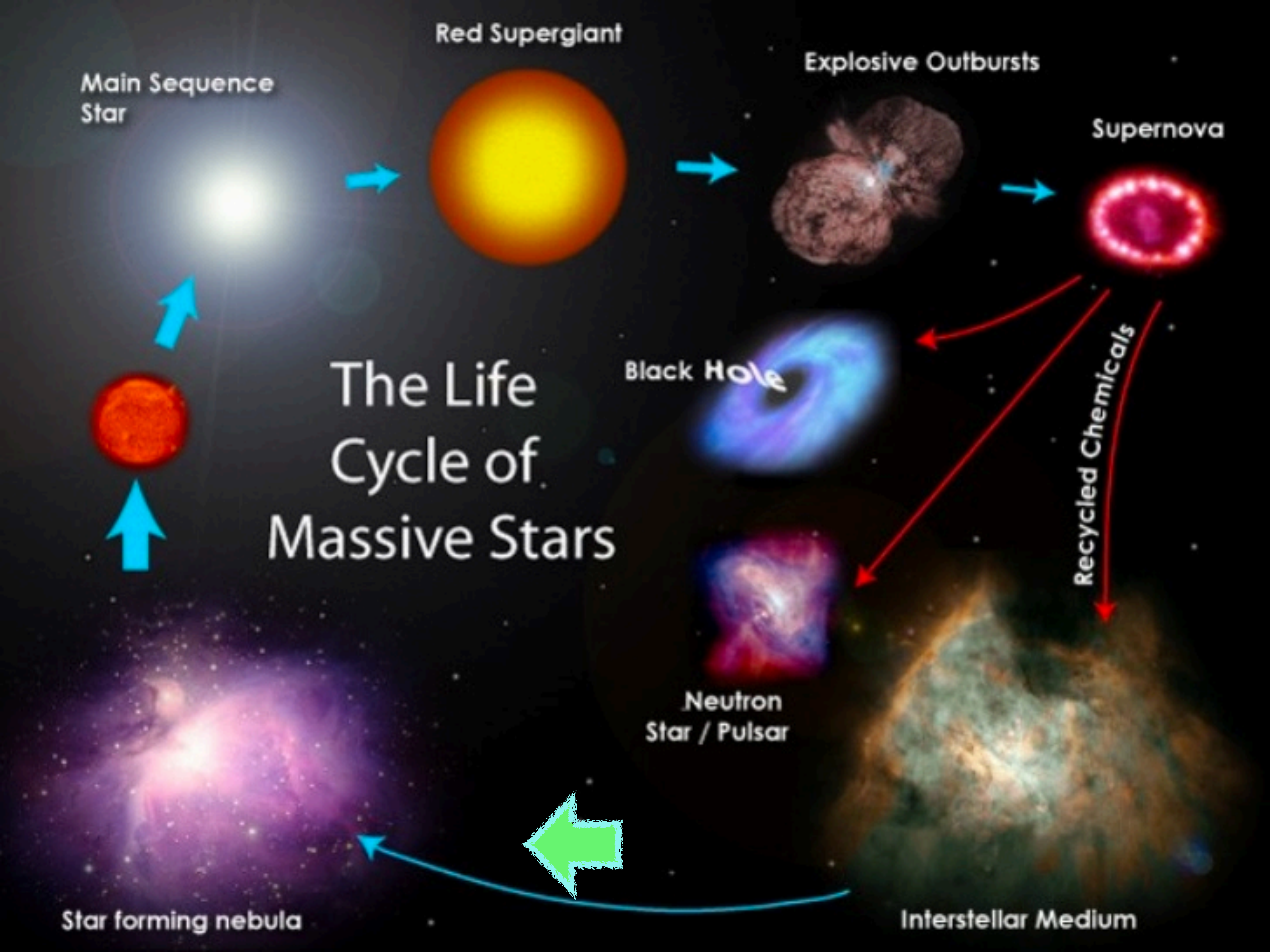
Red Supergiant
Main Sequence Star
Explosive Outbursts
Supernova
Black Hole
The Life Cycle of Massive Stars
Recycled Chemicals
Neutron Star / Pulsar
Star forming nebula
Interstellar Medium

Organization of the Interstellar medium

- Ionized gas (HII)
  - <u>HII regions</u>
  - <u>Warm Ionized Medium (WIM)</u>

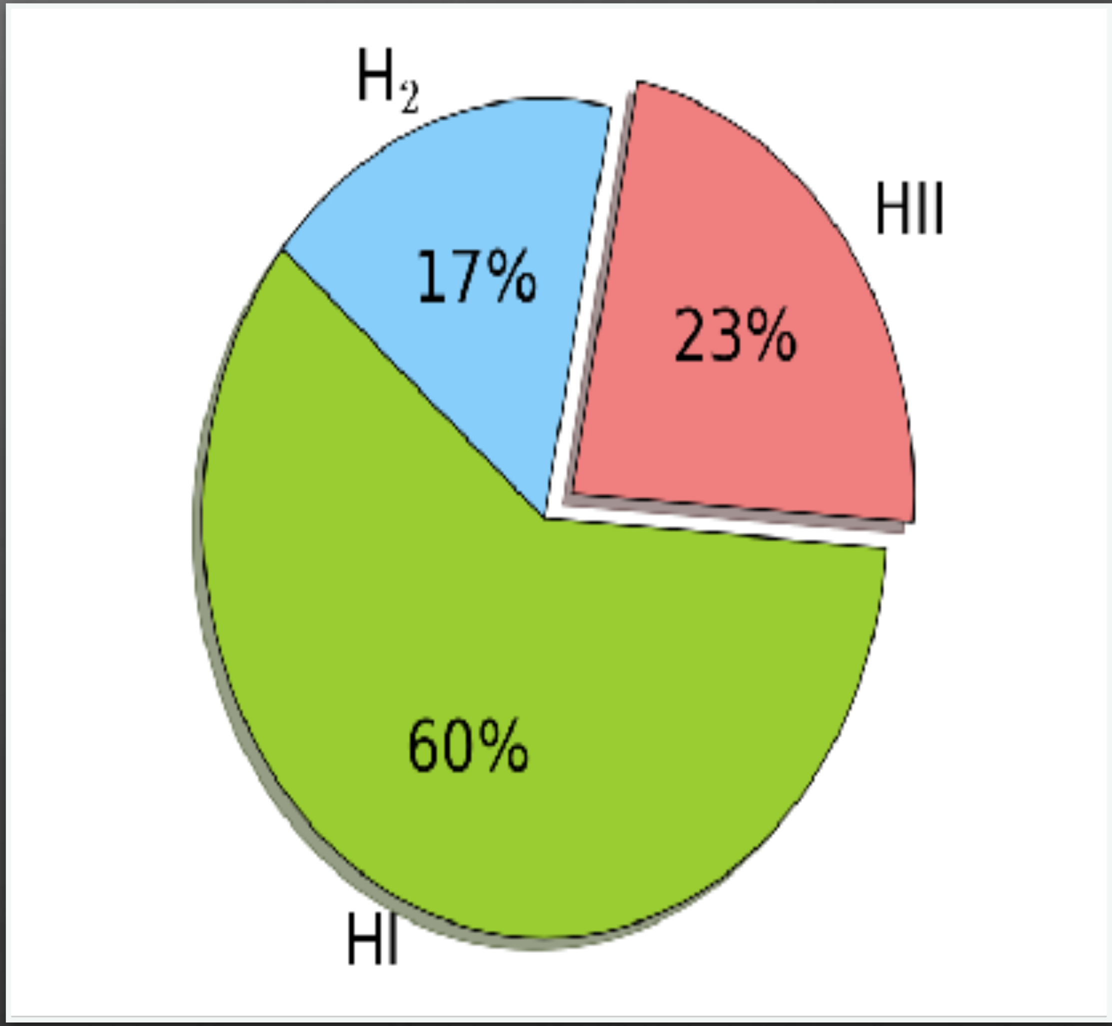

Tracers of the ionized gas

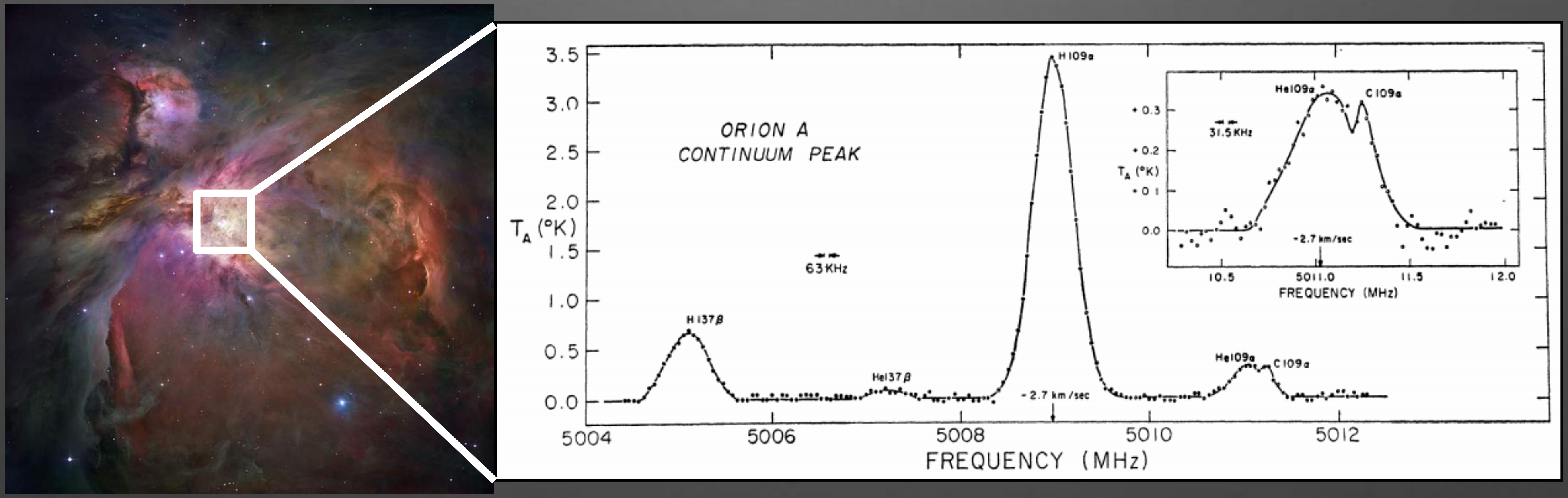

Radio Recombination Line (RRL)

$$\Delta\nu_D \frac{T_l}{T_c} = 2.5\times10^{-12}\left(a^{-1}(\nu, T)\right)T^{-1.15}\nu^{2.1}(6f_{nm}n^{-1})\left(\frac{N(H^+)}{N(H^+ + He^+)}\right),$$

Motivations

★ SIGGMA fully covers the entire Galactic plane observable by Arecibo telescope.

★ The aim is to produce the most sensitive RRL survey ever made of the galactic plane.

Blind survey for RRL emitting regions:

- Search for new HII regions
- Detect carbon RRL from PDRs
- Other possibilities (WIM, SNR etc.)

Comensal Survey with PALFA

Observe 12 alpha lines simultaneously (300 MHz BW total)

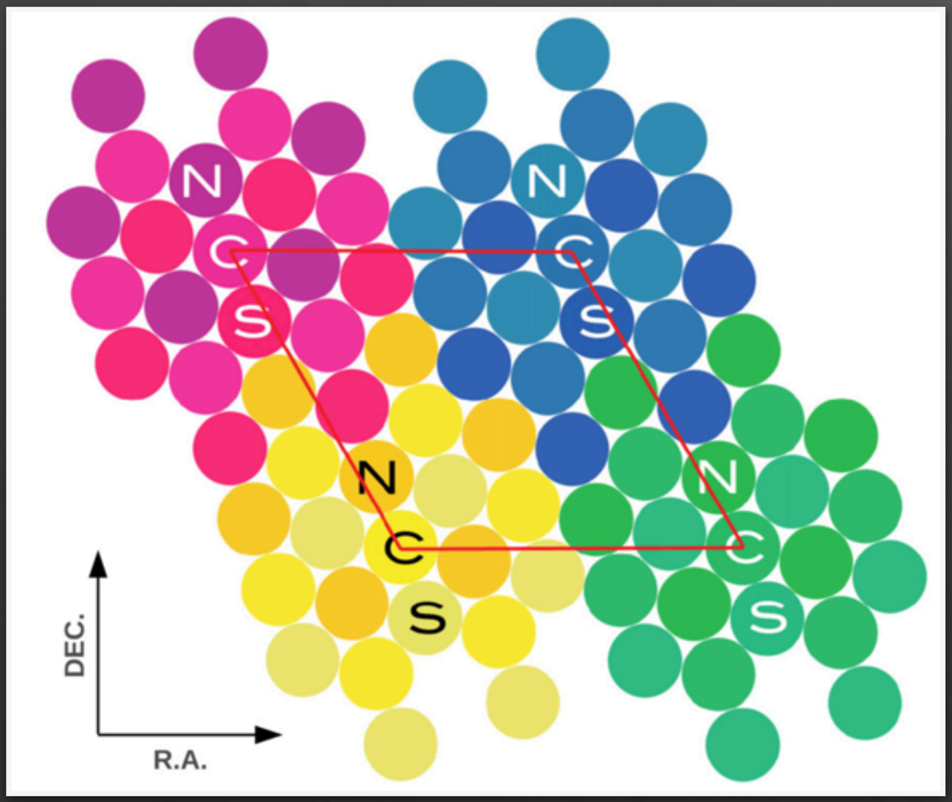

Parameter	Value
l	$32° - 70°$
b	$-1°.5 - +1°.5$
FWHM	$3'.4$
Spectral resolution	$4.2\ \mathrm{km\,s^{-1}}$
Velocity range	-300 - +300 $\mathrm{km\,s^{-1}}$
Integration time	270 s
rms noise	0.65 $\mathrm{mJy\ beam^{-1}}$

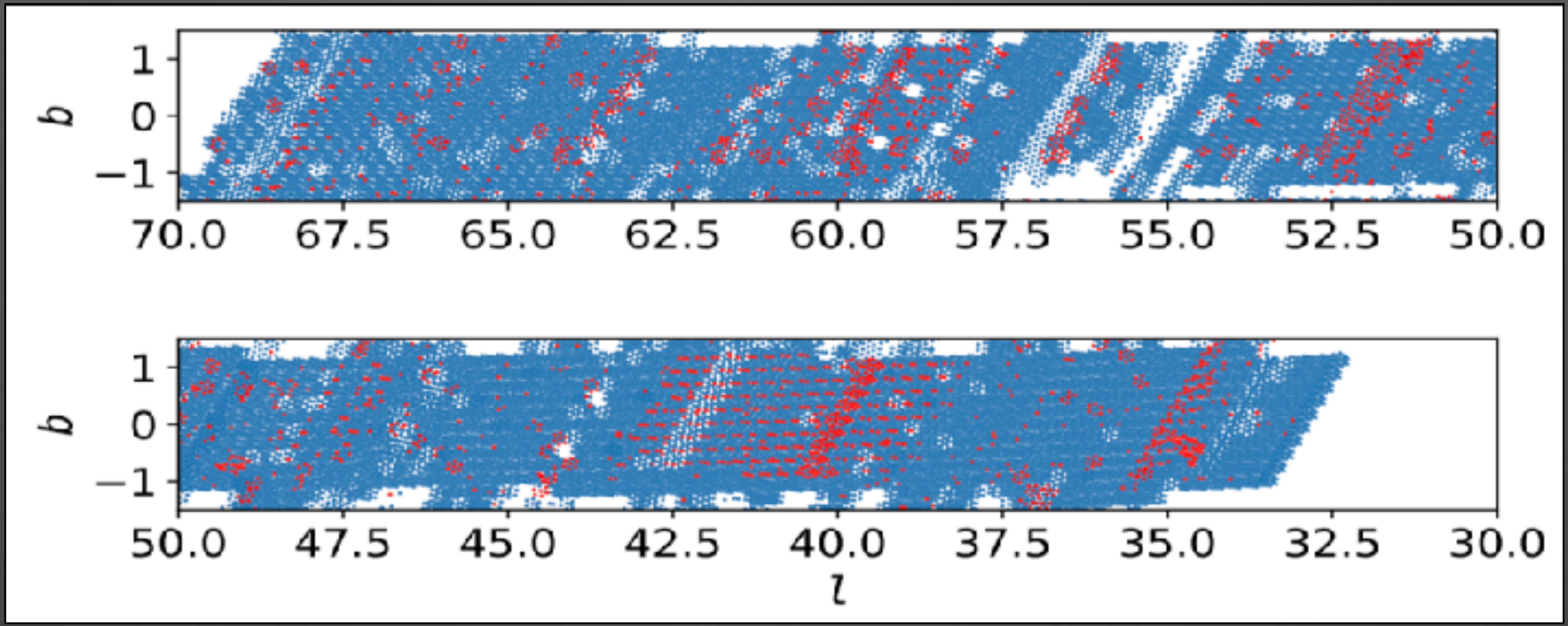

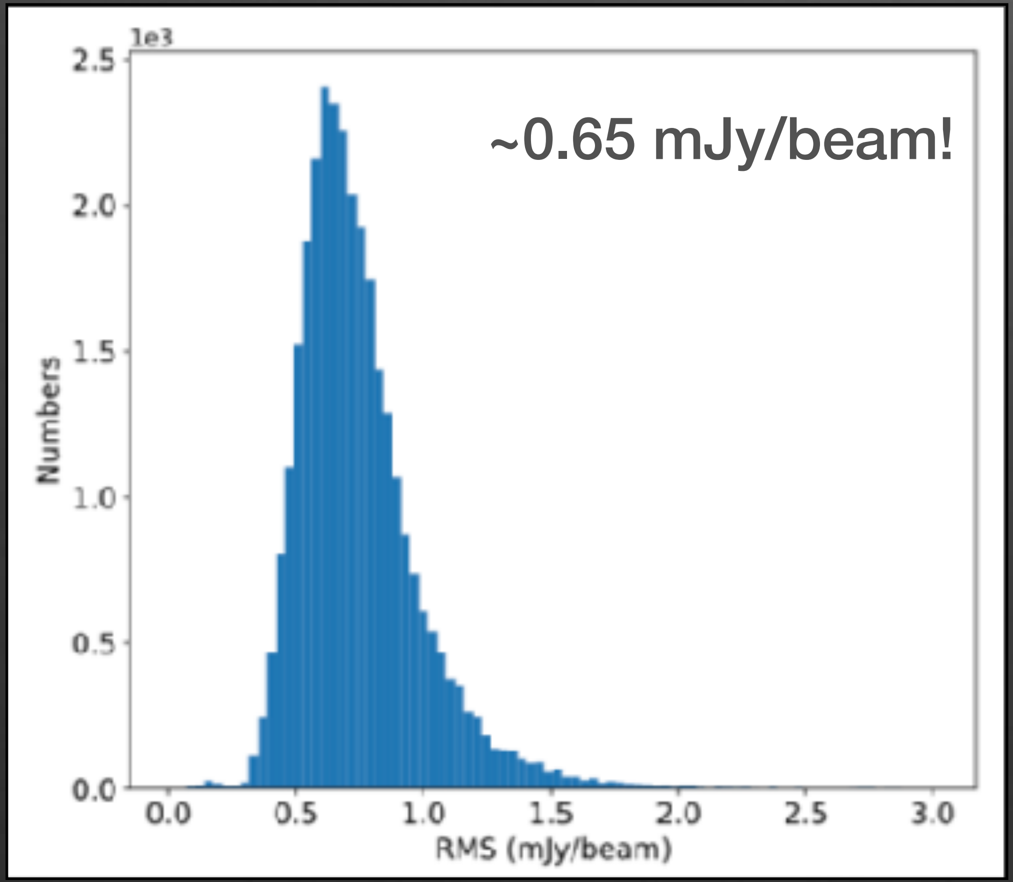

High sensitivity

RFI and baseline problems

Fully sampled (not Nyquist)

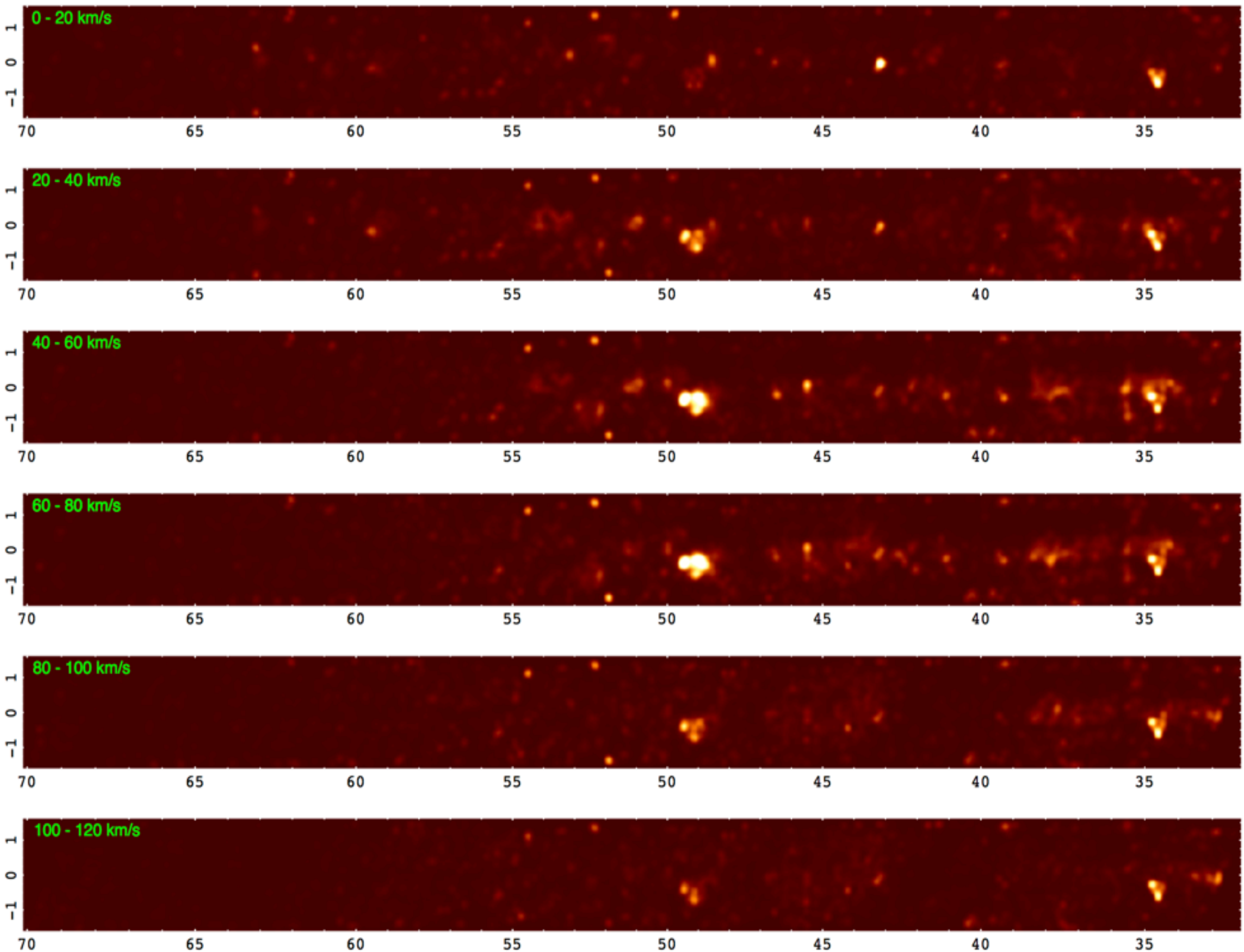
0 - 20 km/s
20 - 40 km/s
40 - 60 km/s
60 - 80 km/s
80 - 100 km/s
100 - 120 km/s
1
0
-1
70
65
60
55
50
45
40
35

l - v diagram comparing with CO data

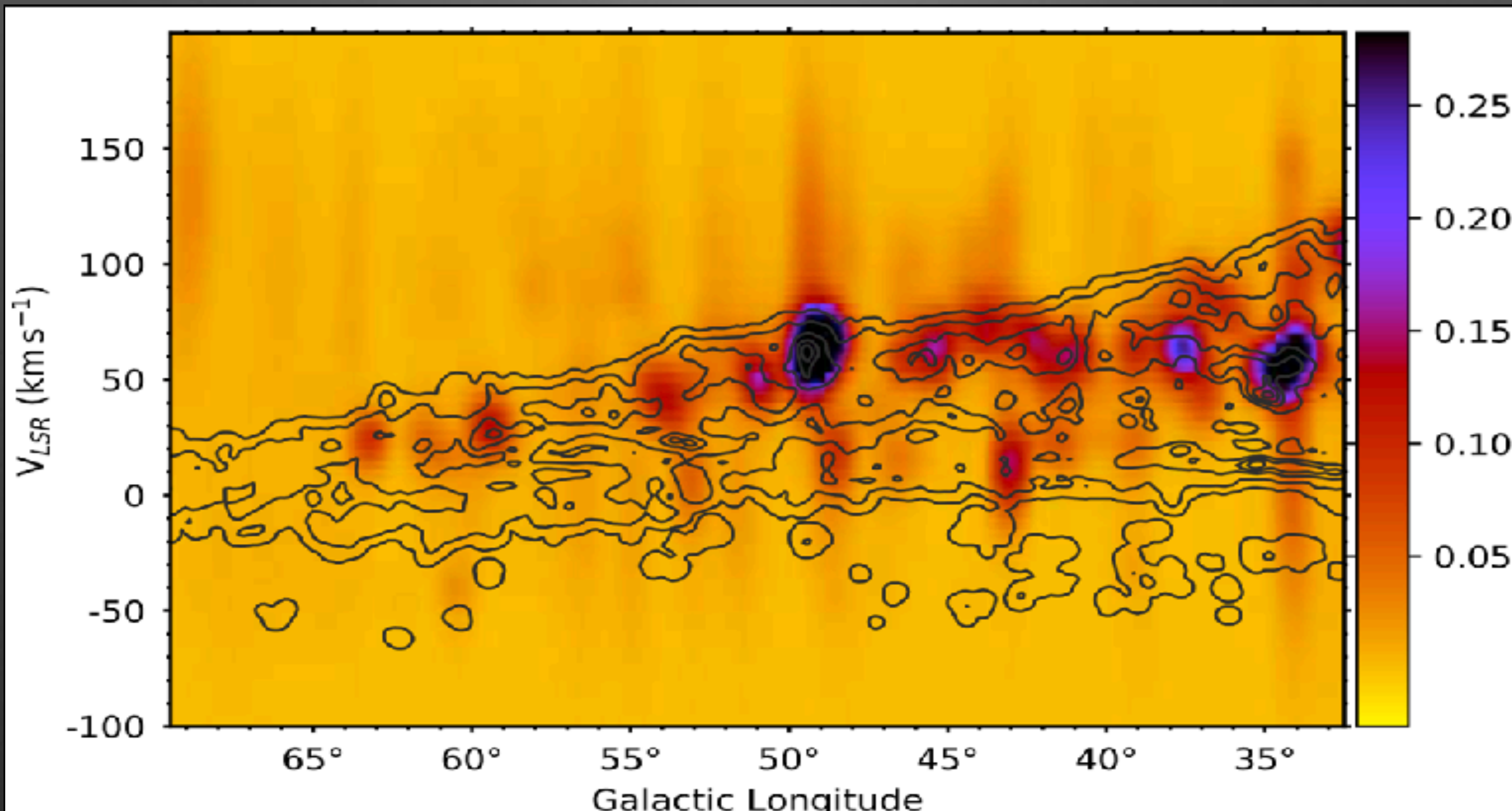

CO contours by Dame et al. 2001

Thermal emission derived from RRL

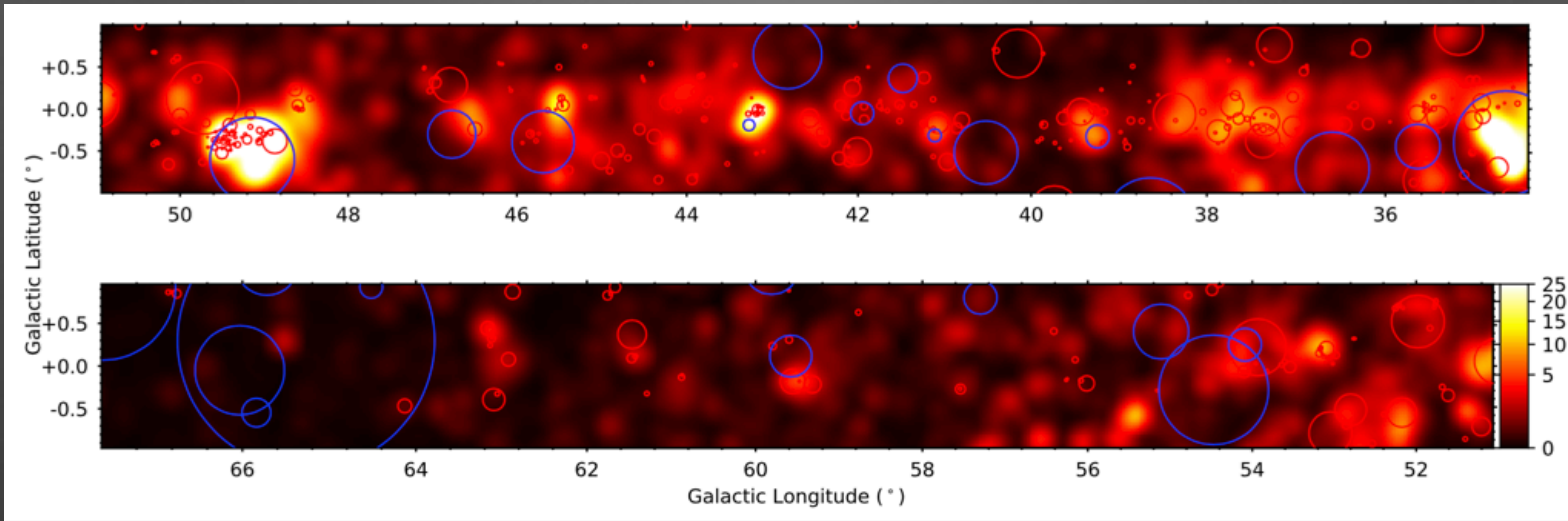

$$T_C = \frac{(1 + 0.08)}{6985} \cdot a(T_e) \cdot T_e^{1.15} \cdot \nu_{GHz}^{-1.1} \cdot \int T_L dV,$$

W49 region

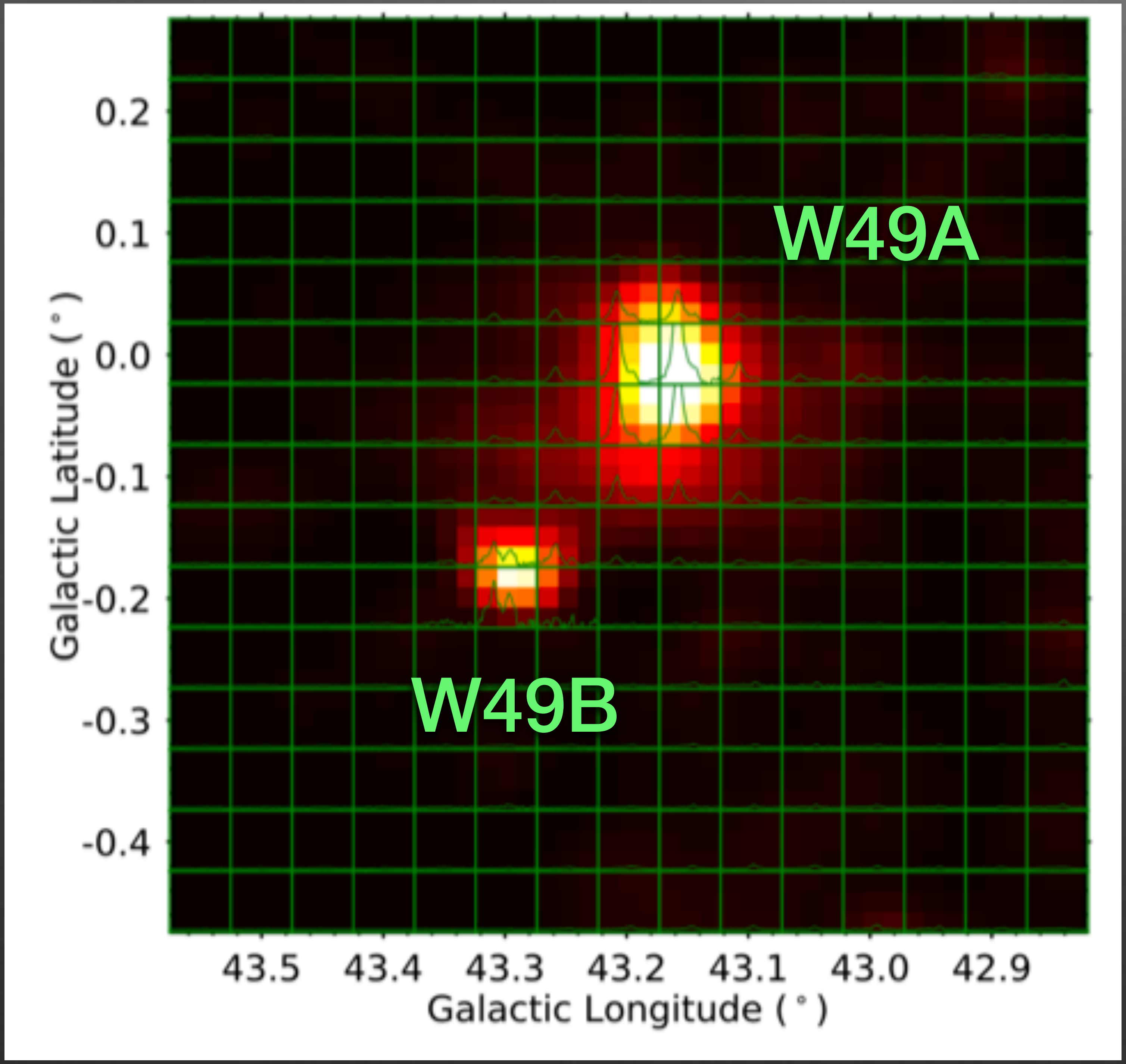

W49A
W49B
0.2
0.1
0.0
-0.1
-0.2
-0.3
-0.4
Galactic Latitude (°)
43.5
43.4
43.3
43.2
43.1
43.0
42.9
Galactic Longitude (°)

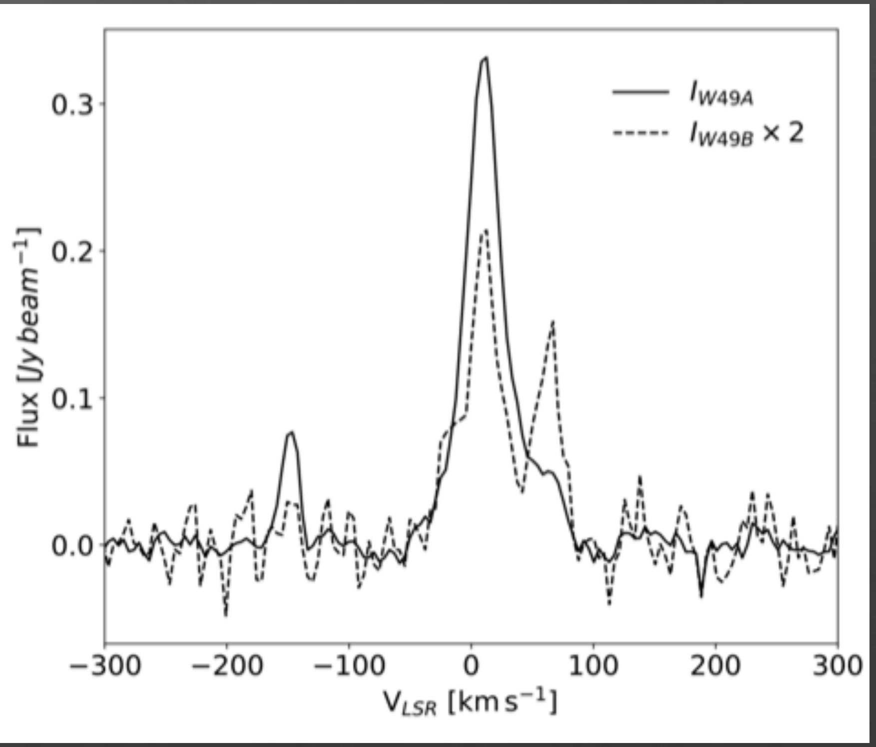

I_{W49A}
$I_{W49B} \times 2$
0.3
0.2
0.1
0.0
Flux [$Jy\,beam^{-1}$]
−300
−200
−100
0
100
200
300
V_{LSR} [$km\,s^{-1}$]

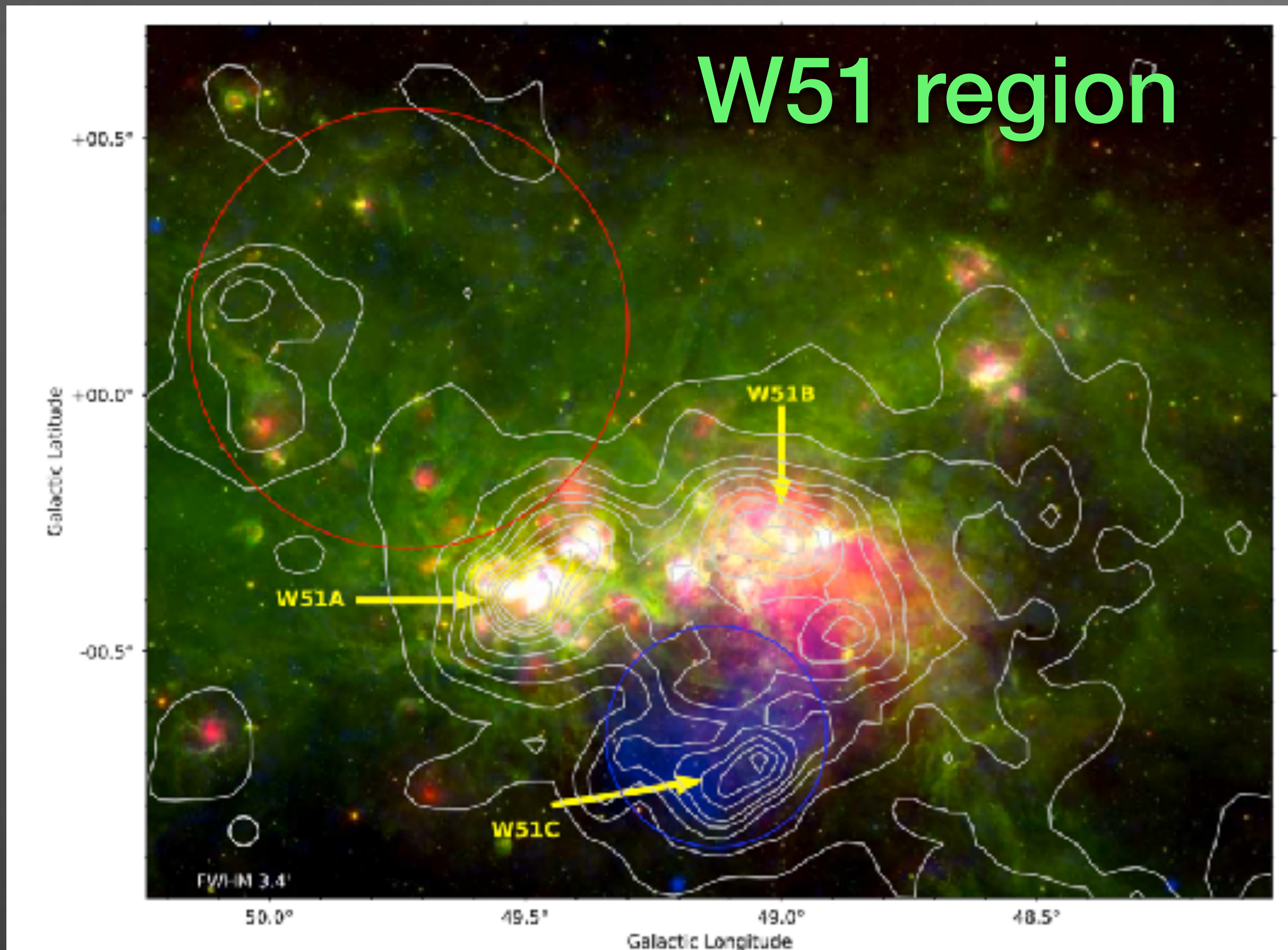

W51 region
W51B
W51A
W51C
FWHM 3.4'
+00.5°
+00.0°
-00.5°
Galactic Latitude
50.0°
49.5°
49.0°
48.5°
Galactic Longitude

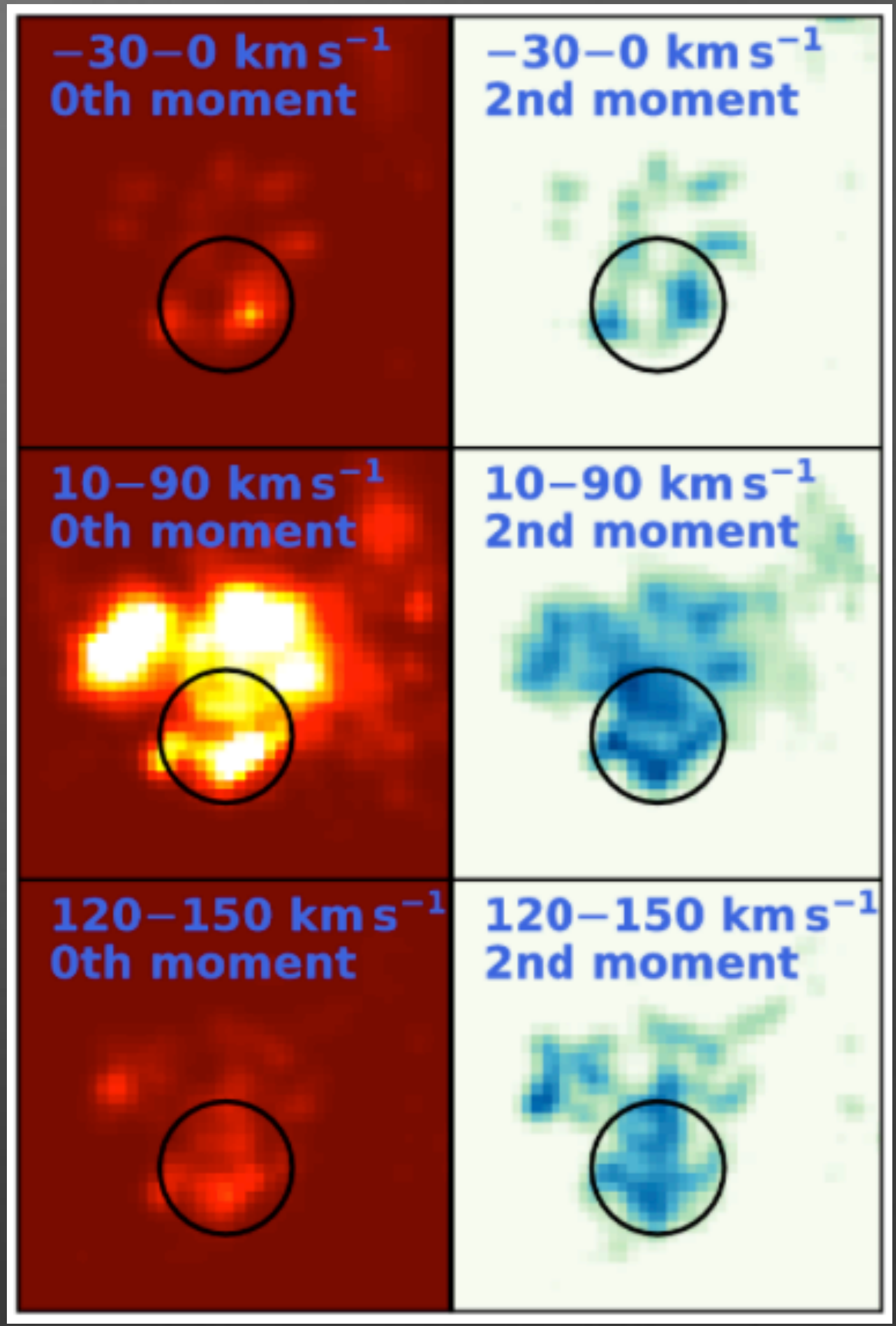

−30−0 km s−1
0th moment
−30−0 km s−1
2nd moment
10−90 km s−1
0th moment
10−90 km s−1
2nd moment
120−150 km s−1
0th moment
120−150 km s−1
2nd moment

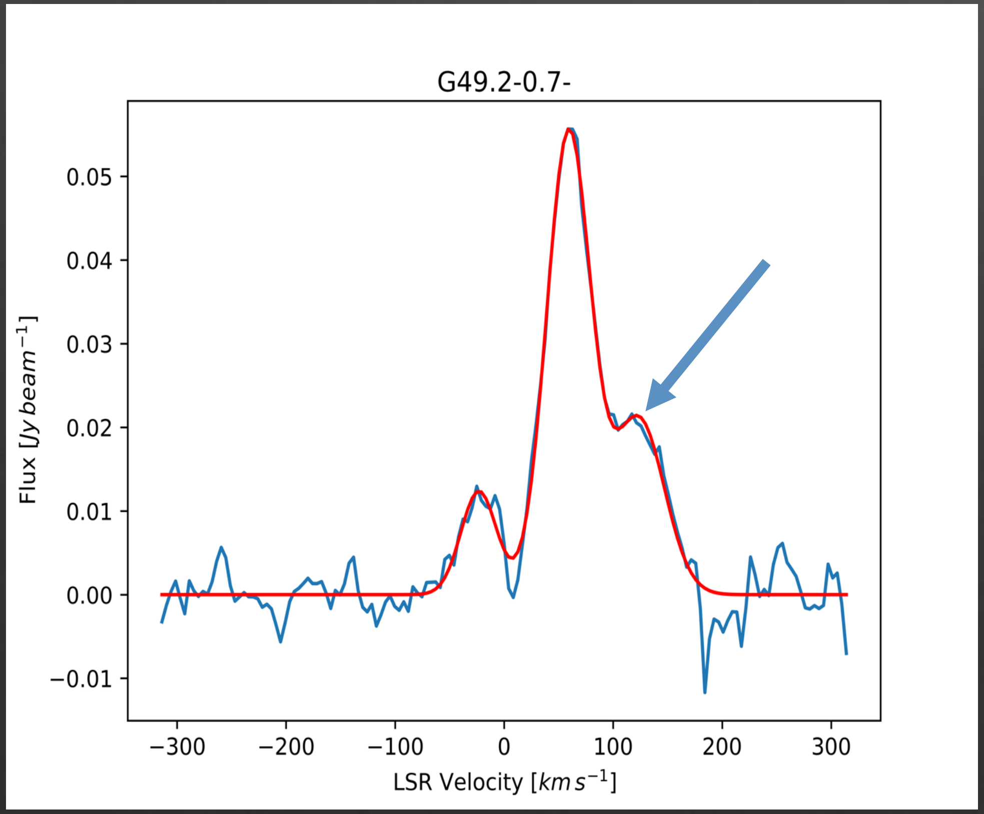

G49.2-0.7-
Flux [Jy beam−1]
LSR Velocity [km s−1]
0.05
0.04
0.03
0.02
0.01
0.00
−0.01
−300
−200
−100
0
100
200
300

SNR: W51C

The RRL catalogues of SIGGMA

RRL detections

- 338 known HII regions
- 84 new HII regions
- 11 carbon RRL regions
- 14 detections towards SNRs

SIGGMA data cubes will be accessible online in 2018!

Name	l	b	Peak	V_{LSR}	FWHM	RMS	S/N
	°	°	mJy beam^{-1}	km s^{-1}	km s^{-1}	mJy beam^{-1}	
G032.800+00.190	32.800	+0.190	9.16 ± 1.01	14.9 ± 1.2	22.1 ± 2.8	1.65	8.9
G032.823+00.072[a]	32.824	+0.072	30.40 ± 2.89	106.7 ± 1.2	25.3 ± 2.8	2.76	19.0

Name	l	b	Peak	V_{LSR}	FWHM	RMS	S/N
	°	°	mJy beam^{-1}	km s^{-1}	km s^{-1}	mJy beam^{-1}	
G033.024−00.366	33.025	−0.366	26.15 ±2.02	50.8 ±1.2	28.2 ±3.0	2.61	18.2

Name	l	b	Radius	H II Region	$\int I_{CRRL} dV$	C/H[a]	Quality[b]
	deg.	deg.	deg.		Jy km s^{-1}		

GName[a]	Other Name	l	b	Radius	V_{LSR}	FWHM	D_N	D_F	D	Quality[c]
		deg.	deg.	deg.	km s^{-1}	km s^{-1}	kpc	kpc	kpc	
G33.6+0.1	Kes 79	33.67	+0.03	0.11	106.3	26.1	6.4	7.5	7.1[1]	C
G34.7−0.4	W44	34.67	−0.42	0.32	47.7	114.3	2.9	10.8	2.9[2]	B
					49.4	11.6	3.0	10.7		
					138.0	80.0	6.8	6.8		
G35.6−0.4		35.60	−0.43	0.13	53.7	23.5	3.2	10.3	3.6[3]	A
G36.6−0.7		36.59	−0.69	0.28	40.6	64.4	2.5	10.8	⋯	B
					57.5	20.2	3.4	9.9		
					146.0	71.5	6.7	6.7		
G39.2−0.3	3C 396	39.23	−0.32	0.08	12.8	34.0	0.8	9.2	≤ 11.3[4]	A
					61.2	24.5	3.7	9.2		
G40.5−0.5		40.51	−0.51	0.23	45.3	36.1	2.8	9.8	⋯	C
G41.1−0.3	3C 397	41.12	−0.31	0.05	62.1	24.5	3.8	8.7	10.3[5]	A
G41.5+0.4		41.46	+0.39	0.12	19.2	18.2	1.3	11.2	10.3[6]	A
G43.3−0.2	W49B	43.27	−0.19	0.07	9.1	42.5	0.6	11.5	7.5[1],10[7]	A
					62.7	24.7	4.1	8.0		
G45.7−0.4		45.56	−0.35	0.21	65.1	18.6	4.8	6.8	⋯	B
					86.5	100.4	5.8	5.8		
G46.8−0.3	HC 30	46.77	−0.27	0.16	60.2	25.3	4.4	7.0	6.4[1]	C
G49.2−0.7	W51C	49.14	−0.61	0.22	62.3	41.2	5.4	5.4	6[1]	A
					122.8	51.8	5.4	5.4		
G54.4−0.3	HC 40	54.47	−0.29	0.38	43.6	15.5	4.1	5.6	3.3[1],6.6[8]	B
G57.2+0.8	4C21.53	57.24	+0.82	0.10	106.1	39.8	4.5	4.5	⋯	B

(Liu et al. 2018, submitted)